Military Technical College
Kobry Elkobbah,
Cairo, Egypt

8th International Conference
on Aerospace Sciences &
Aviation Technology

TURBULENT FLOW STRUCTURE IN A VARIABLE AREA DUCT

A.A. MOSTAFA[1]

ABSTRACT

Turbulent structure of air flow field in a multi-convergent divergent duct is examined experimentally using a hot wire anemometer having an x-probe. The lateral profiles of the normalized mean axial and traverse velocities and the kinetic energy of the mean flow at selected axial stations are presented. The distributions of turbulence root mean square, shear stress, skewness and flatness are also presented. The present results improve the understanding of the interaction between the mean flow and turbulent quantities with periodic changes of flow cross-sectional area. This understanding is quite essential for the optimum engineering use of multi-convergent divergent ducts in either MHD or enhancement of heat transfer applications. The experimental data are also useful for developing suitable turbulence and numerical sub-models for prediction of the flow fields in variable area ducts.

Keywords: Aerodynamics, variable area duct, hot wire measurements, convergent divergent duct, mean flow-turbulence interaction.

1. INTRODUCTION

Turbulent flow in variable area ducts is of practical importance. Power generation units, air conditioning ducts, heat exchanger devices, and conveying ducts are just few examples. In the area of magneto hydrodynamics (MHD), converging diverging ducts were the subject of many fruitful basic studies [7]. Figure 1 shows the diffuser section of a MHD duct where the two diverging sides represent the insulators while the two-parallel sides simulate the electrodes.

In the mean time, some devices such as circular rings and vane swirlers are inserted in plain tubes to augment heat transfer coefficient [1]. These devices disturb or break down the boundary layer and hence augment the heat transfer.

[1]Associate professor, Mechanical Power Dept., Faculty of Engineering, Cairo University, Giza, Egypt

From this prospective, multi-convergent divergent ducts might be good candidates for the enhancement of heat transfer processes without excessive pressure drop.

Close analysis of previous studies of MHD and heat transfer augmentation indicates that most of these studies focused on mean flow characteristics. However, the increase in transport quantities of these studies is due to the increase of turbulent diffusion caused by random motion of turbulence eddies. Therefore, a deeper insight into the interaction between the mean flow and turbulence quantities with the effect of area changes seems essential for optimum engineering design.

Nowadays, numerical solution of highly complicated turbulent flows is becoming a design tool for many engineering applications [10,14&16]. However, correct predictions of such complex flows require the use of an accurate turbulence model [4&19] along with a generalized body-fitted grid system [9&17]. The development of such physical and numerical sub-models is always hindered by the lack of well-defined data sets that accurately report detailed mean and turbulent flow variables. This is because the performance of numerical and physical sub-models is highly affected by inlet boundary conditions [20&21]. The present measurements document the traverse distributions of all primitive variables at the starting plane of the test section.

In the present paper, detailed hot wire measurements of mean flow field and turbulence quantities in a multi-convergent divergent duct are reported. The flow variables at the starting plane of the test section as well as the distributions at other eight axial stations are measured. The selected configuration reduces the effect of inlet conditions compared with the effect of area variation on mean and turbulent flow quantities. The present results clarify the effects of area changes on flow structure and highlight the interaction between mean flow and their associated turbulence quantities.

2. TEST RIG

Figure 2 shows the test section and system of coordinates. Air is supplied to the test section through an air blower, a filtration unit, a supply pipe, a bypass valve, a control valve and an orifice meter. Before entering the test section, air is passed through a smooth aluminum rectangular duct having a length (L) of 0.9 m, a height (H) of 0.075 m and a width (2b) of 0.04 m. At the entrance of this duct, a honey comb mesh was inserted to straighten the flow. As shown in Fig. 3, the test section consists of six subsections forming three complete cycles. Each divergent subsection starts with a flow width of 0.04 m and ends with 0.06 m. As thus, the diffuser subsections have a wall angle of 5.7° with the x-axis and a maximum area ratio of 1.5. The relatively small angle and area ratio are selected to minimize the possibility of having flow separation in the diffuser subsections. The measurements are performed at the horizontal midway plane between bottom and top sides. The traverse distributions of the flow variables are measured at nine axial stations, including the starting plane, shown in Fig. 3. Horizontal slots in the upper plate are made to allow the insertion of the probe while the unused slots are covered during measurements. A computer-

controlled two-dimensional traverse mechanism is used to move the x-wire probe in the x and y directions.

Simultaneous time resolved velocity in the x and y directions are measured with an x-wire probe. Two hot wires (5 μm diameter Pt-10% Rh, 1.25 mm length each) are mounted orthogonally in the x-y plane. Each wire length to diameter ratio is large enough to neglect end conduction effects. The hot wire system is of the constant temperature anemometer type made by Dantic Company [3] and is recently used by Enayet et al. [5]. The main components of this system are the probe, the bridge, the main unit, the hardware signal processing module and a personal computer. A computer software is used to drive a fully automated two-dimensional traverse mechanism and to perform the data processing. Description of the hot wire technique, its accuracy and limitations and its advantages in measuring turbulent flow fields are reported in the literature [2 &15] and will not repeated here.

3. RESULTS AND DISCUSSION

The measured mean velocity components at the inlet plane of the test section are presented first to highlight the inlet conditions and to clarify the accuracy of the present measurements. Distributions of the flow variables within the first diffuser subsection are then presented. After that, measurements at geometrically similar axial stations are compared with each other to show the effect of the preceding cross-sectional area variation on the measurements. Throughout the whole presentation, the flow variables are normalized using the centerline velocity at the test section entrance plane (U_c) and the traverse distance is normalized by half the duct width at the same plane (b). All experimental data are represented by symbols while curve fittings of these data are represented by lines (except in Fig. 4a, the line represents the seventh power law).

Figure 4 presents the traverse profiles at the test section entrance plane. This figure shows that the mean axial velocity and kinetic energy of the mean flow (M.K.E.) are symmetrical while the traverse mean velocity is skew-symmetrical about the duct centerline. In turbulent flow regime, the mean axial velocity component can be represented by the relation $U = U_c(1 - y/b)^{1/n}$. The value of n depends on the Reynolds number, which is equal to 4.2×10^5 in the present study. The solid curve in Fig. 4a shows the distribution of U/U_c with the value of $n = 7$. The discrepancy between the seventh power law and the present data might be attributed to the present Reynolds number which is relatively high. As indicated by Mostafa [13], a value of $n = 7.5$, gives the best fit of the mean flow data considered in his work. As shown in Fig. 2, air flows through a straight duct of length to width ratio of 22.5 before entering the test section. This configuration allows the traverse profiles at the test section entrance plane to approach the shape of fully developed flow [11]. As demonstrated in previous studies [2&15], the accuracy of hot wire measurements can be estimated by the ratio of the traverse to axial velocity in a fully developed flow. As thus, Fig. 4 indicates that the accuracy of the present measurements is quite acceptable. Fig. 4b shows that the traverse mean velocity is skew-symmetrical about the duct centerline with zero value at the centerline and it is of the order of two

percent of its corresponding axial component. This distribution is consistent with the mean velocity profiles presented in Fig. 4a and indicates that the geometrical centerline coincides with the flow centerline. As thus, the rest of the results are presented over half of the duct width only.

Figure 5 presents the traverse distributions of the normalized mean quantities at Sts. 1, 2 and 3. It should be noted that St. 2 has a 25 % increase in flow cross-sectional area compared with that at St. 1, while St. 3 has a 50 % increase. The effect of adverse pressure gradient or the increase in cross sectional area on the mean flow is clear as can be seen from Fig. 5a. It shows that the values of mean streamwise velocity at St. 3 are smaller than the corresponding ones at St. 1, especially near the wall. The U/U_c profile presented in Fig. 5a indicates that turbulent flow in the diffuser subsection can generally be divided into three major flow regimes. The first region is near the diffuser centerline, which corresponds to an inviscid core region where the influence of the wall is relatively small. The typical decrease in the centerline mean velocity with x in this region is seen in Fig.5a. The second regime is the near wall region which is similar to the near-wall flow of a turbulent boundary layer subjected to a severe adverse pressure gradient [18]. The third region, between the core and the boundary layer, represents a highly distorted turbulent flow with large variations in the U-velocity gradients. In this region, the turbulence levels and rate of turbulence production and dissipation are greatly in excess of their corresponding values of a zero-pressure-gradient boundary flow [18 &22]. Figure 5b compares the mean traverse velocity distributions at Sts. 1, 2 and 3. It shows positive traverse velocity that increase with the increase of the flow area. However, the highest value is still about 7% of U_c. This distribution indicates that the mean traverse flow motion is from the core to fill-up the expanded flow area near the wall. The nearest to the wall measured mean streamwise velocity, at St. 3. is about 14 % of U_c (see Fig. 5a). The kinetic energy of the mean flow at that point is almost negligible compared with that of the centerline (Fig. 5c). This observation reflects the tendency of boundary layer separation and formation of reversed flow region near the test section corners. This is in agreement with previous studies of plane diffusers [8,11,12,18&22]. These studies concluded that appreciable flow stall can not be seen when the diffuser wall has a small divergence angle and short length. The experimental results of Kline et al. [8] can be expressed by the correlation:

$$\text{Log}\,(2\theta) = 1.65 - 0.76\,\log\,(l_d/2b) \qquad (1)$$

where θ is the divergence angle and l_d is the diffuser length. At certain θ, with $l_d/2b$ greater than that given by this correlation, the boundary layer separates from the wall. The flow then becomes unsteady and asymmetry with large-scale vortices that fluctuate along and across the mean flow. The wall angle of the present diffuser subsections is not large (5.7°) and moreover the maximum $l_d/2b$ is only 2.5. According to Eq. (1), at $\theta = 5.7°$, $l_d/2b$ should be greater than 6 to encounter any appreciable separation. Based on this analysis, it is not expected to have a circulation or flow stall in the present diffuser subsections. However, and because of the very wide angle of the corner (about 169°), it is expected to encounter a recirculation region of a small size at the duct corners. As indicated in the discussion of Fig. 5a, this region is not captured in the measurement course and was not the focus of the present study.

In the mean time, Mobarak et al. [12] reported measurements of a two-dimensional diffuser of a wall angle of 5°, which is nearly the same as the angle of the present diffuser subsections. They used both a hot wire anemometer and five-hole pressure probe to measure the velocity field. The measurements were taken at six cross-sections distributed along the diffuser axis which are equivalent to x/2b = 0.0, 0.55, 1.67, 2.78, 3.89, and 5. At these stations, they did not encounter any reversed flow. As thus, the present results are in agreement with the experimental findings of Kline et al. [8] and Mobarak et al. [12].

Figure 6 presents the traverse distributions of the normalized r.m.s. values of the velocity components, the ratio of the lateral to streamwise r.m.s. values and the shear stress. It can be seen from this figure that u/U_c values increase with the increase of the flow area. The increase of u/U_c at the centerline reflects the increase of turbulent transport into the core region as the cross sectional area increase. Fig. 6b indicates that the values of v/U_c do not change much with the increase of the duct area. This might be attributed to the relatively small turbulence production terms of V, which are proportional to the value of V itself. Examination of Fig. 6c shows that v/u varies from 0.4 to 0.7. It also shows that v/u decreases with the increase of flow cross-sectional area. This means that the energetic turbulence eddies become less isotropic further downstream. The normalized turbulence shear stress is shown in Fig. 6d. This figure shows that the highest value is located near the wall region where high level of turbulence is generated. It also shows that the peak value of $\overline{uv}$ increases with increasing flow cross-sectional area until it reaches up to 2.5 times the value of straight duct flows. This increase in $\overline{uv}$ value near the wall reflects an augmentation of transport processes and suggests the use of divergent subsections in heat exchanger applications.

The skewness and flatness of velocity fluctuations are useful in understanding the coherent structure of turbulent flows. The normalized skewness is computed as:

$$U,s = \frac{1}{T}\int_0^T [(U(t)-U)^3/u^3]\,dt \quad \text{and} \quad V,s = \frac{1}{T}\int_0^T [(V(t)-V)^3/v^3]\,dt \tag{2}$$

The normalized flatness seen in Fig. 7 is computed as:

$$U,f = \frac{1}{T}\int_0^T [(U(t)-U)^4/u^4]\,dt \quad \text{and} \quad V,f = \frac{1}{T}\int_0^T [(V(t)-V)^4/v^4]\,dt \tag{3}$$

where U(t) and V(t) are instantaneous velocities, t is the time, and T is the averaging time. The skewness measures the symmetry of the probability density function (PDF) while the flatness measures the deviation of the PDF of the velocity profile compared with a Gaussian PDF profile. Flatness higher/lower than 3 indicates considerable velocities having higher/lower values than the mean velocity. This means the existence of thicker/thinner tails than that of Gaussian PDF profile. Skewness of zero means a symmetric PDF of a homogeneous-isotropic turbulence for small and large scale eddies (i.e., ideal turbulence in a box) [6]. Results in Fig. 7 show large variations of U,s, V,s, U,f and V,f over y/b at different stations. It also indicates that the location of the measuring station has a great effect on these parameters, especially at the centerline. Figure 7 also shows large non-zero skewness (both

positive and negative) and flatness far from 3. The results presented in Fig. 7 may explain the limitations of turbulence models, which assume isotropic turbulence in predicting complex flows [11&15]. The discrepancies between the predictions (obtained by k-ε model where k is the kinetic energy of turbulence and ε is its dissipation rate) and the experimental data of the same geometry used in the present work reaches up to fifty percent at the boundary layer edge near the duct walls [11].

Figures 8-10 assess the change of the flow due to area variation. In these figures, the distributions of the normalized mean and turbulence quantities as well as higher turbulence moments are presented at Sts. 6 and 8. St. 6 is in the middle of a divergent subsection while St. 8 is in the middle of a convergent subsection, see Fig. 3. Figure 8a shows that the centerline value of U/U_c at St. 8 is smaller than the corresponding value at St. 6. This behavior reflects the more lateral uniformity of U/U_c distribution within the convergent subsection compared with that in the divergent subsection. Figure 8b shows that V/U_c is positive over the whole cross-section of St. 6 while it is negative at St. 8. This means that the flow moves away from the centerline towards the duct walls within the diverging subsection while it moves towards the centerline within the converging subsection. However, the non-zero V value at the centerline at St. 6 (also in Figs. 5b & 11b) reflects an experimental error that might be attributed to little deviation between the measuring location and geometrical axis. It should be noted that the hot wire equations for the effective cooling velocities could give the direction of V with respect to the y-coordinate. This can be done provided that the x-wire probe is in the correct direction for U provided $U \neq 0$. The x-wire measurements are not valid only if the direction of U is not known which is not the case in the present study. The normalized kinetic energy distributions presented in Fig. 8c show that the mean flow has higher kinetic energy at St. 6 than that of St. 8. However, St. 8 has higher values in the near wall region.

Figure 9 compares the second order moments at Sts. 6 and 8. This figure indicates that both u/U_c and v/U_c increase almost linearly with the traverse distance until their highest values at the edge of the boundary layer. Fig. 9c shows that the ratio of v/u ranges from 0.5 (close to the wall) to 0.65 (at the centerline). The shear stress distribution reported in Fig. 9d indicates that St. 6 has higher shear stress than that of St. 8. This distribution is consistent with the mean velocity profiles presented in Fig. 8 which reflects that St. 6 has higher velocity gradients than those at St. 8 (especially in the wall region) and hence higher turbulence levels. The peak value of $\overline{uv}$ at St. 6 is almost five times of the corresponding value at St. 8. This result proposes the use of shorter length of the convergent part than that of the divergent subsection. In this way, the length of the convergent subsections, with low turbulent diffusion, are reduced and its function will be just to flatten the velocity profile or decrease the boundary layer thickness before entering a new divergent subsection.

Figure 10 presents the variation of higher order moments with the traverse distance at Sts. 6 and 8. It can be seen from this figure that the variation of the higher order moments over the lateral distance is larger than that of St. 8. This observation indicates that the turbulence at St. 8 which is located in the middle of the convergent subsection is more isotropic or homogeneous than that at St. 6 which is in the middle of the divergent subsection.

Figures 11-13 present the traverse distribution of the normalized flow variables at three geometrically similar stations of equal areas, Sts. 1, 5 and 9. As thus, any differences in the flow variables might be attributed to the flow history, which is controlled by the ability of the fluid particles to adjust their dynamics caused by the preceding geometry. St. 1 is preceded by a long straight duct, while Sts. 5 and 9 are located between convergent and divergent subsections. As thus and as might be expected, Fig. 11 indicates that the mean quantities at Sts. 5 and 9 are closer to each other compared to those at St. 1. The large-scale structure can be visualized from the sign of V shown in Fig. 11b. This Figure shows positive lateral mean velocity at St. 1 which might be attributed to the existence of a divergent subsection downstream St. 1. In contrast to the expectations of vanishing lateral velocity component at the throat cross-sectional areas, Fig. 11b shows negative lateral mean velocities. This means that the effects of convergent subsections preceded Sts. 5 and 9 overwhelm the effects of the divergent subsections downstream these stations. Fig. 11c indicates that the maximum kinetic energy of the mean flow at St. 9 is not at the centerline, similar to St. 1, but rather is located in the highly distorted region between the core and boundary layer regions.

Figure 12 indicates that u/U_c at Sts. 5 and 9 are smaller than the corresponding values at St. 1. In contrast to this, Fig. 12b shows the v/U_c values at Sts. 5 and 9 are higher than those of St. 1. The distribution of v/u, in Fig. 12c, has the general characteristics of the distributions of both u/U_c and v/U_c shown in Fig. 12a&b. As thus, Fig. 12c indicates that the large scale or energetic eddies are more isotropic (v/u closer to one) at Sts. 5 and 9 compared with those at St. 1. The distributions presented in Fig. 12d indicate that the level of shear stress at St. 1 is slightly higher than that of Sts. 5 and 9. This behavior of the cross-correlation $\overline{uv}$ is consistent with the less isotropic turbulence encountered at St. 1 when compared with the turbulence levels at Sts. 5 and 9 (see also Fig. 12c).

Figure 13 presents the traverse distributions of the skewness and flatness at Sts. 1, 5 and 9. This figure shows that the values of V,s are relatively larger than that of U,s. The same is true for V,f and U,f which is consistent with the existence of the lateral spreading of strong large-scale coherent eddies in the lateral direction.

4. SUMMSRY AND CONCLUSIONS

Detailed measurements of turbulent flow field in a multi-convergent divergent duct are presented. These data are obtained using a hot wire anemometer having an x-probe. Results at the entrance plane and eight other selected downstream stations of the test section are presented and analyzed. The conclusions that can be drawn from the present study are summarized as:

1. The increase in the flow cross-sectional area creates a mean lateral fluid motion, which results in thicker boundary layer. This change in the mean flow increases the r.m.s. in the streamwise direction. Therefore, turbulence eddies become less isotropic or homogeneous when compared with those of straight duct flow.
2. The energetic large-scale turbulence eddies are less isotropic with lower coherent structure near the wall than those in the core region.

3. The throat cross-sectional areas have more homogeneous turbulence than that at the entrance plane of the test section, which is preceded by a straight duct.
4. The upstream geometrical configuration effect on the flow structure is higher than that of identical downstream configuration. This emphasis the importance of inlet boundary conditions even for elliptic problems. This point explains the failure of k-ε model, which is based on the local isotropy assumption to predict diffuser flows.
5. The shear stress and hence the turbulent diffusion level in diffuser subsections are much higher than that encountered in convergent subsections. This observation may be considered in the implementation of multi-convergent divergent ducts in heat exchanger applications.

NOMENCLATURE

b	: test section half width at the entrance plane, m
MHD	: magneto hydrodynamics
M.K.E.	: mean kinetic energy of the mean flow = $0.5(U^2 + V^2)$, m^2/s^2
r.m.s.	: root mean square of the velocity fluctuations, m/s
St.	: measuring station
Sts.	: measuring stations
u,v	: root mean square of the velocity fluctuations in the streamwise and traverse directions, respectively, m/s
$\overline{uv}$	: turbulence shear stress, m^2/m^2
U,V	: mean velocities in the streamwise and traverse directions, respectively, m/s
U(t), V(t)	: instantaneous velocities in the streamwise and traverse directions, respectively, m/s
U_c	: mean streamwise velocity at the centerline of the entrance plane, m/s
U,f, V,f	: normalized flatness of velocity fluctuations in the streamwise and traverse directions, respectively
U,s, V,s	: normalized skewness of velocity fluctuations in the streamwise and traverse directions, respectively
x, y,z	: cartesian coordinates
θ	: wall divergence angle with the x-axis

REFERENCES

1. Abdel-Salam, M.S., Khalil, E.E., Mostafa, A.A., and Mostafa, G.M., "An Experimental Optimization of Using Vane Swirlers to Augment Heat Transfer Performance in Turbulent Swirling Tube Flow," the 5th Int. Conference of Fluid Mechanics, Cairo, (1995).
2. Brown, L.W.B., Antonia, R.A. and Chua, L.P., "Calibration of x-probes for turbulent flow measurements," Experiments in Fluids, Vol.7, pp.201-208 (1989).
3. Dantic Electronics, "Dantic 56c01 CTA Instruction Manual," Denmark, (1987).
4. Correa, B.M., and Shyy, A.D., "Computational Models and Methods fo Continuous Gaseous Turbulent Flows," Progress in Energy and Combustion Systems, Vol. 13, pp. 249-292, (1987).
5 Enayet, M.M., Khalifa, M.M., and Mostafa, A.A., "An Experimental Study of

Turbulent Flow in a Two Dimensional Zigzagged Passage," J. of Engineering and Applied Science, Faculty of Engineering, Cairo University, Vol. 44, No. 5, pp. 975-987, (1997).

6. Hinze, J.O., "Turbulence,", Mcgrawhill company, Newyork, (1967).
7. Kamiyama, S.I., "Analysis of Two-Phase MHD Flow in Converging-Diverging Ducts," Paper presented at the 4th Beer-Sheva Seminar on MHD Flows and Turbulence, Ben-Gurion University of the Negev, Beer-Sheva, Israel, (1984).
8. Kline, S.J., Johnston, J., and Pand Reneau, L.R., "Performance of Straight two-Dimensional Diffusers," J. of Basic Engg., (1967).
9. Lee, D., and Yeh, C.L., "Computation of Turbulent Recirculating Flows Using Hyprid Adaptive Grid," Numerical Heat Transfer: Part A: Applications, Vol. 26 pp. 415-430, (1994).
10. Lin, C.A., and Lu, C.M., "Modeling of Three-Dimensional Gas-Turbin Combustor Model Flow Using Second-Moment Closure," AIAA J., Vol. 32, pp. 1416-1422, (1994).
11. McMillan, O.J., and Johnston, J.P., "Performance of Low-Aspect-Ratio Diffusers With Fully Developed Turbulent Inlet Flows, Part II: Development and Application of a Performance Prediction Method," J. Fluids Engg., Trans. ASME, pp. 393-400, (1973).
12. Mobarak, A., Fouad, M.A., and Metwally, M.A., "Turbulence Measurements in a Straight Walled Two Dimensional Diffuser," ASME paper 86-GT-60, (1986).
13. Mostafa, A.A., "Turbulent Flow in a Multi-Divergent Convergent Duct," 8th Int. Applied Mechanics and Mechanical Engineering Conference, Military Techanical College, Cairo-Egypt, (1998).
14. Ogut, A., Yoshida, T., and Brian, R., "CFD Analysis of Flow in a Turbopump Diffuser with Wall Suction," Adv. Comp. Methods in Fluid Dynamics, ASME, Fluids Engg. Div, Vol. 196, pp. 295-315, (1994).
15. Perry, A.E., "Hot-wire anemometry," Clarendon Press, Oxford, (1982).
16. Sharif, M.A.R., and Wong, Y.K.E., "Evaluation of the Performance of three Turbulence Closure Models in the Prediction of Confined Swirling Flows," Computers and Fluids, Vol. 24, pp. 81-100, (1995).
17. Shy, G.W., Tong, S.S., and Correa, S.M., "Numerical Recirculating Flow Calculations Using a Body-Fitted Coordinate System," Numerical Heat Transfer, Vol.8, pp.99-113, (1985).
18. Trupp, A.C., Azad, R.S. and Kassab, S.Z., "Near-Wall Velocity Distributions within a Straight Conical Diffuser," J. Experiments in Fluids, Vol.4, pp. 319-331, (1986).
19. Wei, H., and Chen, C.P., "Assessment of Advanced Turbulence Models for Recirculating and Swirling Flows," Proceeding of the 1997 ASME Fluids Engg. Div., Summer Meeting, Vancouver, Canada., (1997).
20. Xia, J.L., Smith, B.L., Benim, A.C. Schmidli, J., and Yadigaroglu, G., "Effect of Inlet and Outlet Boundary Conditions on Swirling Flows," Computers and Fluids, Vol. 26, pp. 811-823, (1997).
21. Yaras, M.I., "Effects of Inlet Conditions on the Flow in a Fishtail Curved Diffuser with Strong Curvature," J. Fluids Engg., Vol. 118, pp. 772-778, (1996).
22. Yuan, M., "Two-dimensional Simulation of the Flows in Plane-Wall Diffusers," J. Hydrodynamics, Vol. 4, No. 4, pp. 43-53, (1992).

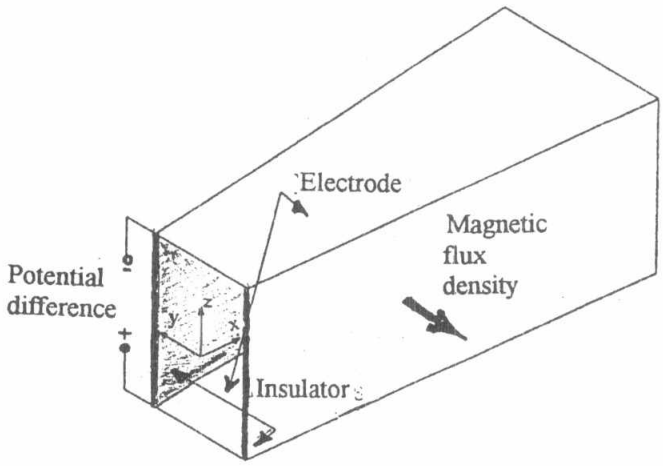

Fig. 1 Diverging portion of MHD [7].

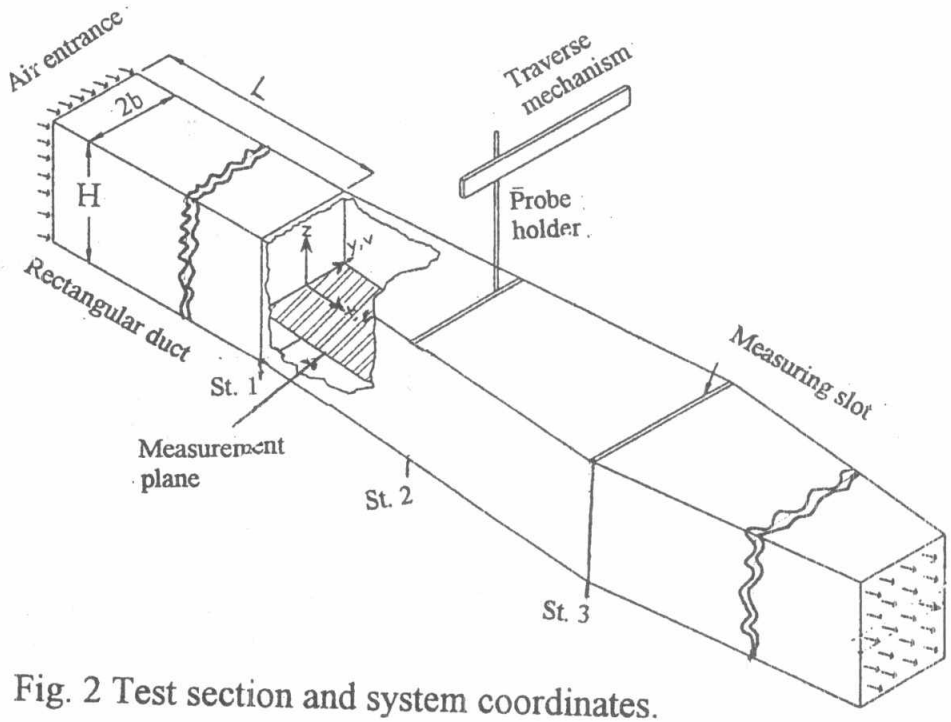

Fig. 2 Test section and system coordinates.

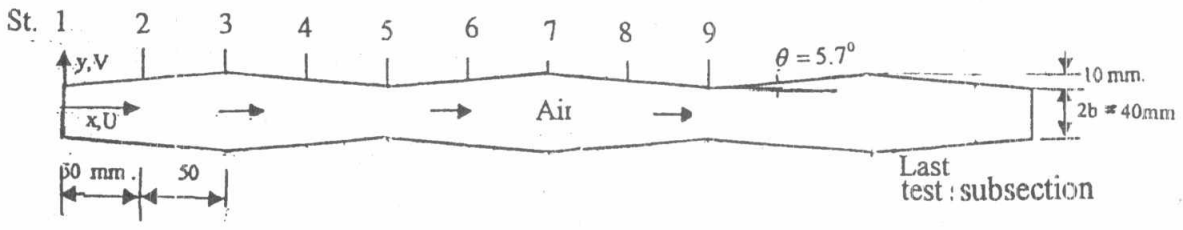

Fig. 3 Axial location of measuring stations.

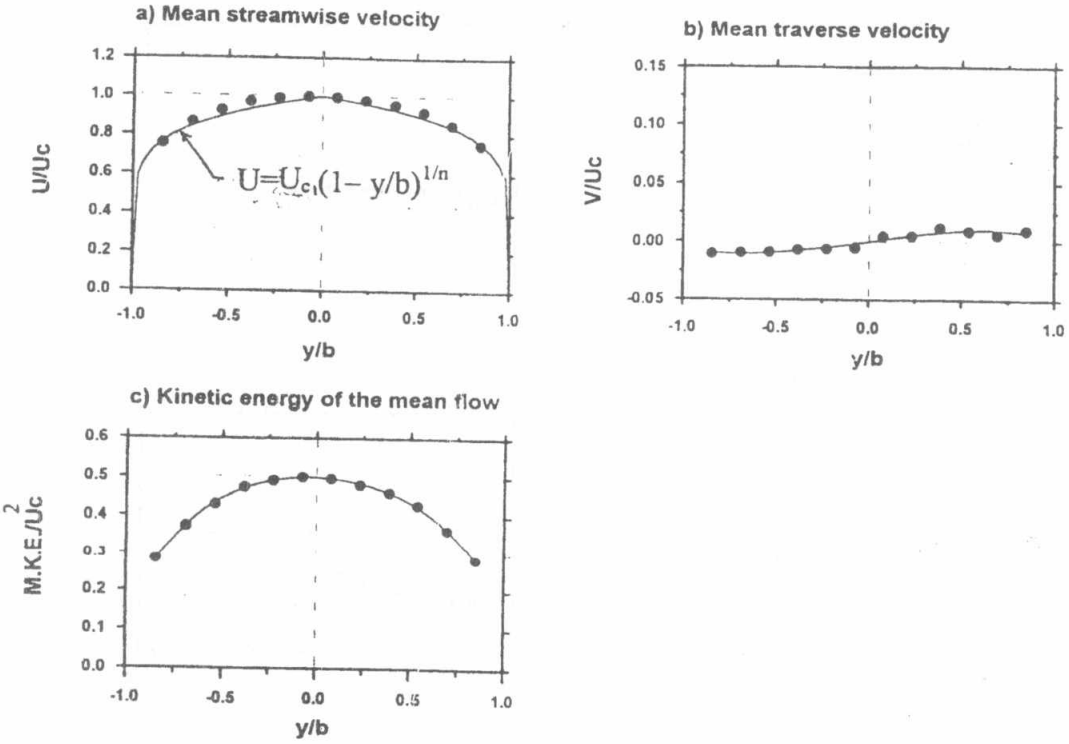

Fig. 4 Traverse distribution of normalized mean quantities at the entrance plane.

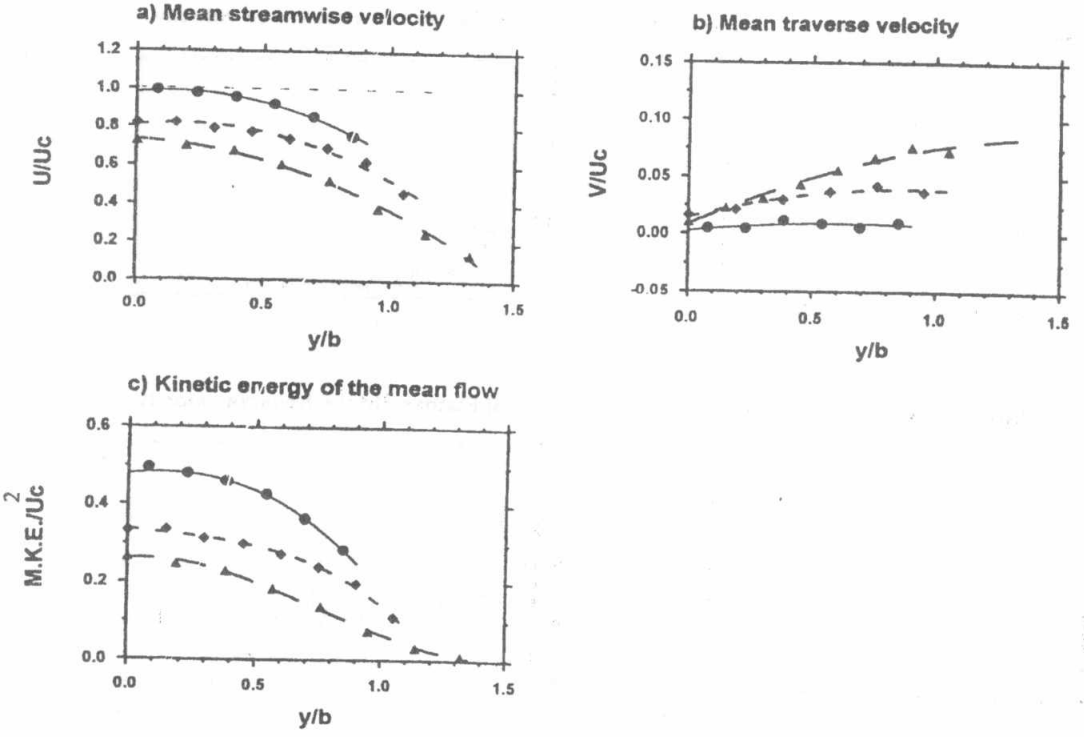

Fig. 5 Traverse distribution of normalized mean quantities at St. 1 (—●—), St. 2 (- -●- -) and St. 3 (—▲—).

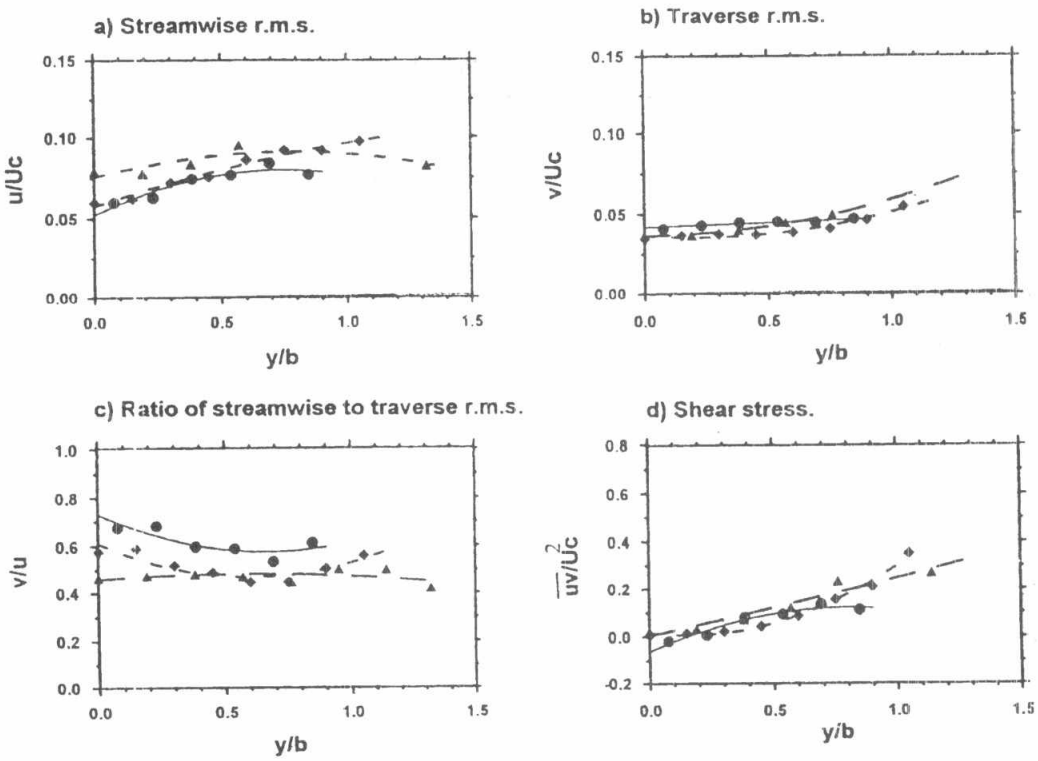

Fig. 6 Traverse distribution of turbulence quantities at St. 1 (—●—), St. 2 (- - ◆ - -) and St. 3 (— ▲ —).

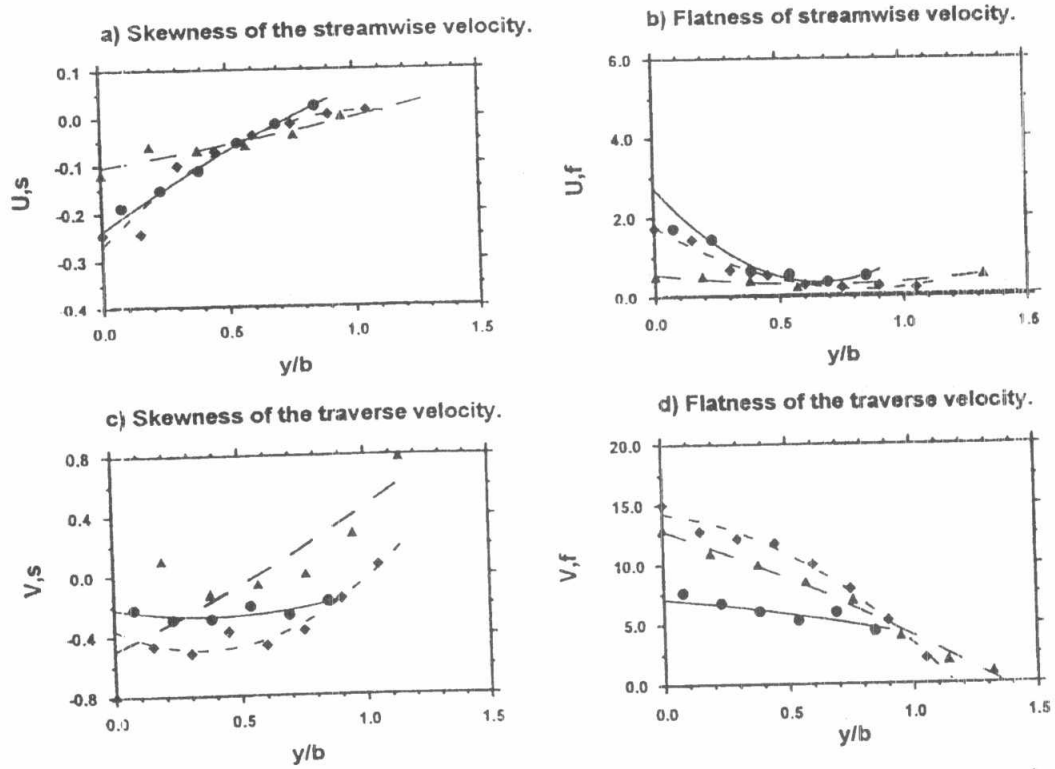

Fig. 7 Traverse distribution of skewness and flatness at St. 1(—●—), St. 2 (- - ◆ - -) and St. 3 (- —▲— —)

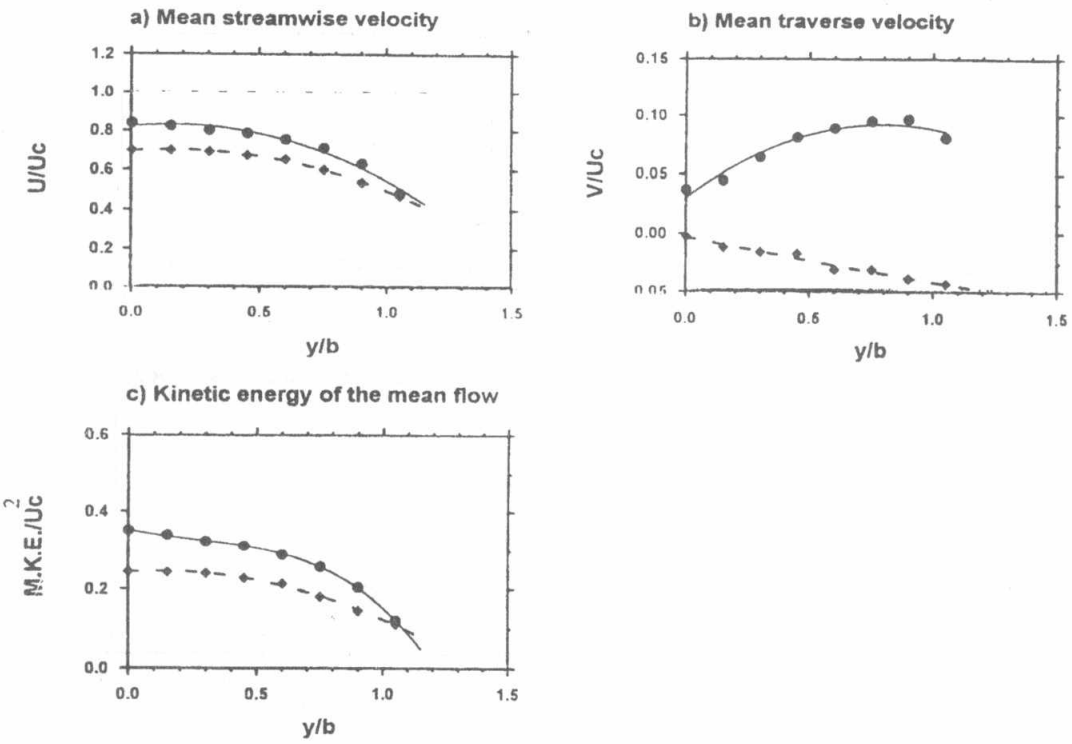

Fig. 8 Traverse distribution of normalized mean quantities at St. 6 (—●—), and St. 8 (- -♦- -) .

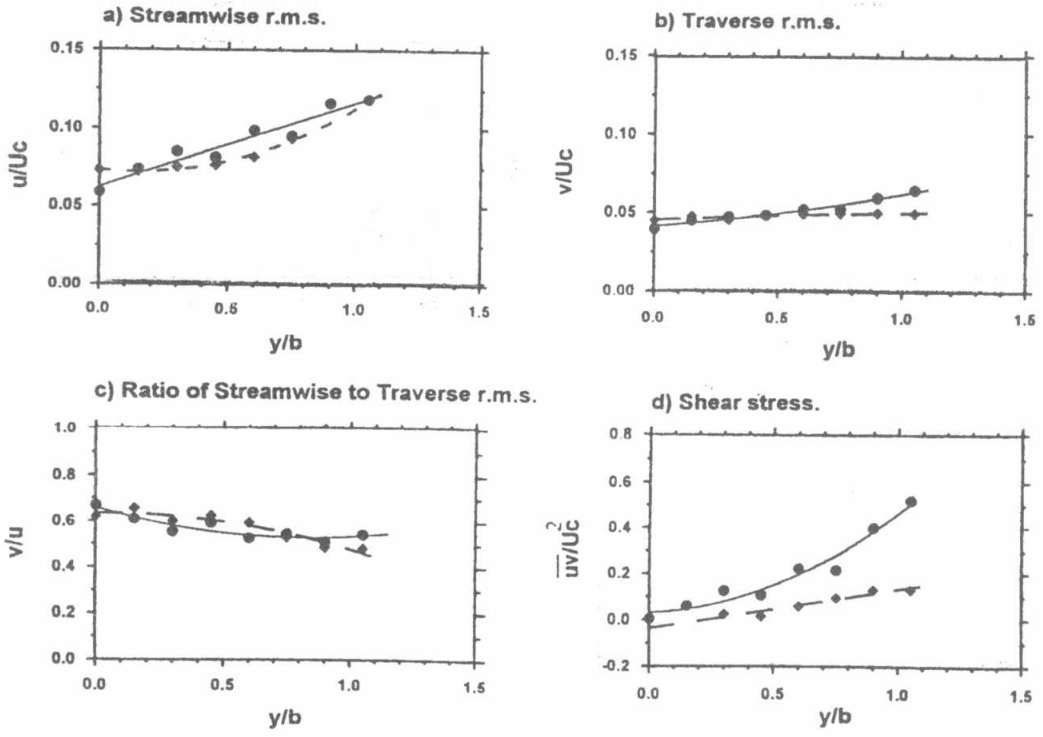

Fig. 9 Traverse distribution of turbulence quantities at St. 6 (—●—) and St. 8 (—♦— —).

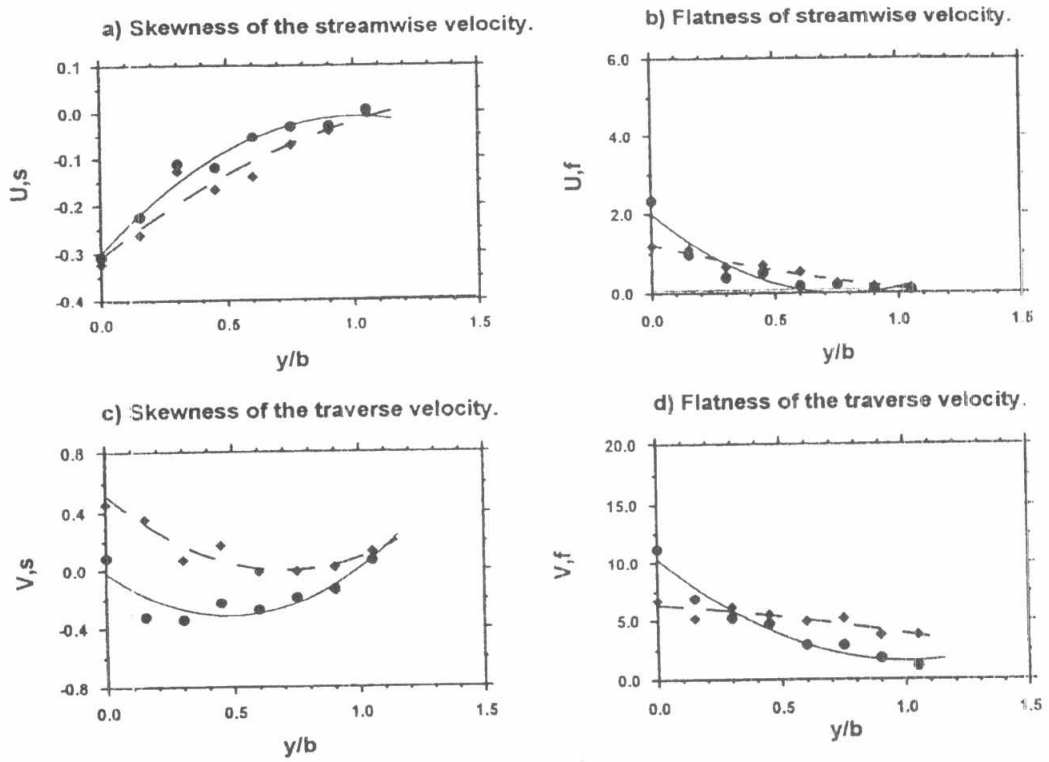

Fig. 10 Traverse distribution of skewness and flatness at St. 6 (– – • – –) and St. 8 (– —•— —)

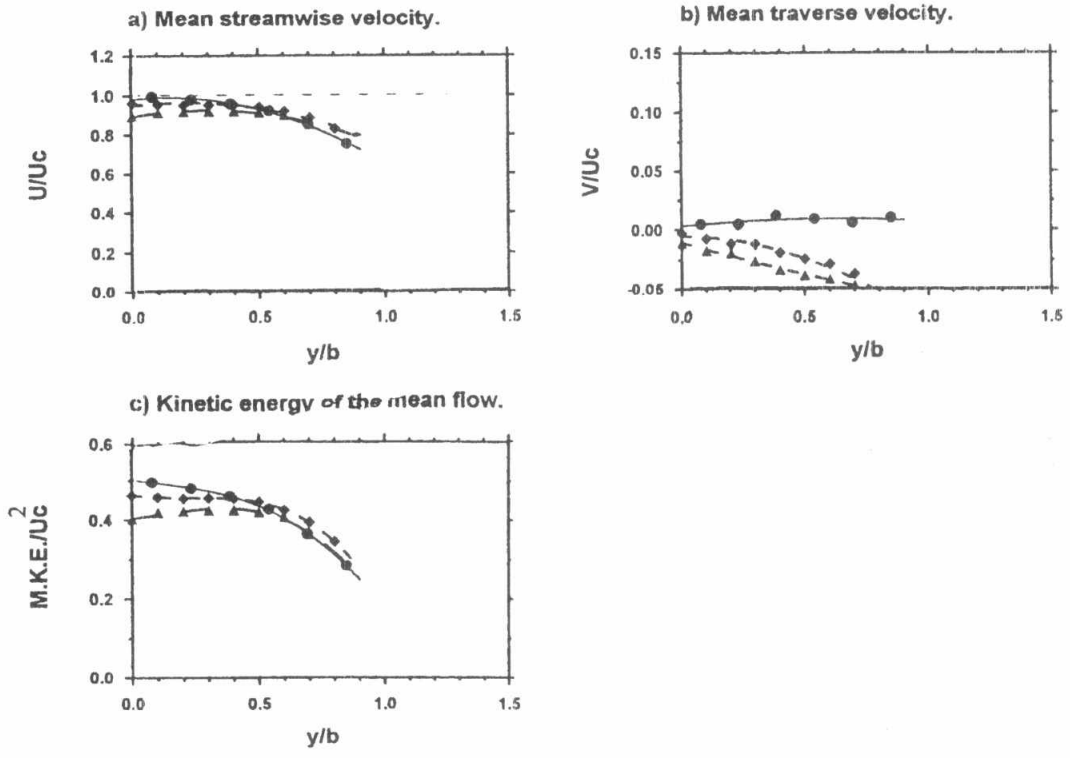

Fig. 11 Traverse distribution of normalized mean quantities at St. 1 (—•—), St. 5 (– – • –), and St. 9 (—▲—).

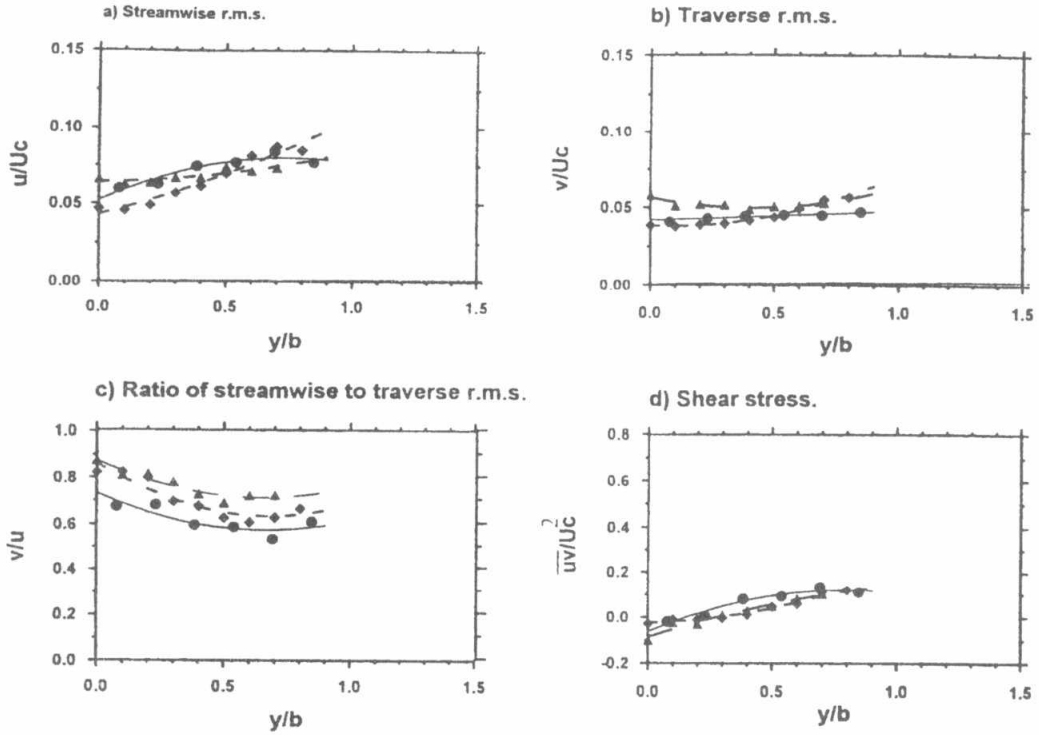

Fig. 12 Traverse distribution of turbulence quantities at St. 1 (—●—), St. 5 (- - ◆ - -) and St. 9 (— ▲ —).

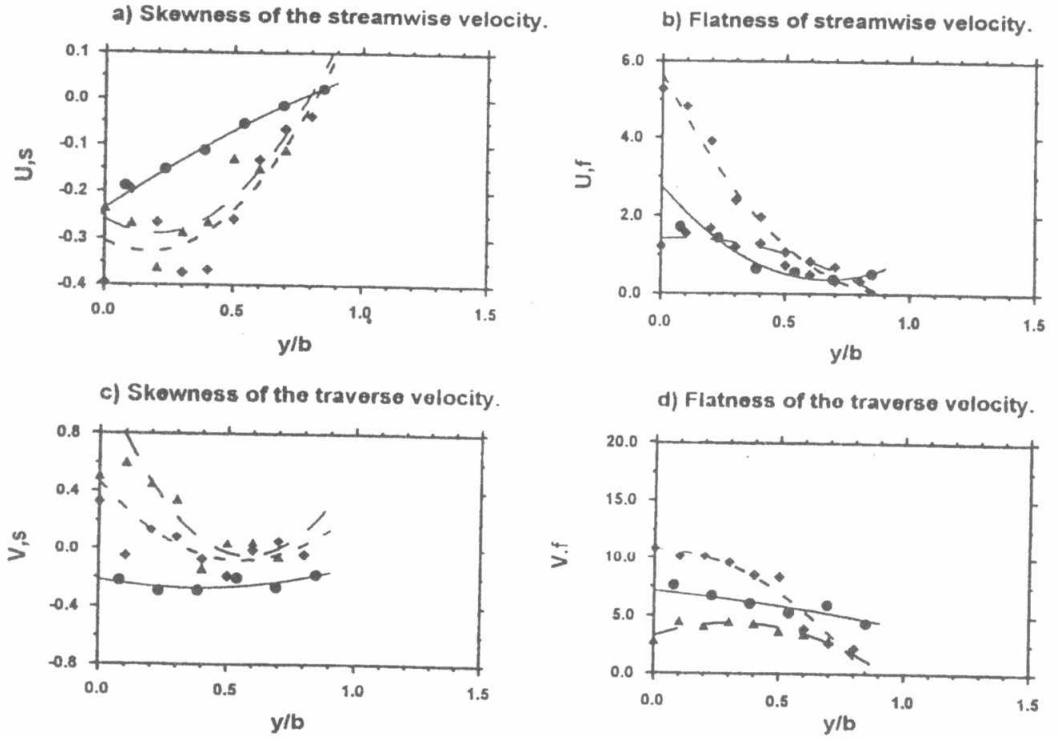

Fig. 13 Traverse Distribution of Skewness and Flatness at St. 1(—●—), St. 5 (- - ◆ - -) and St. 9 (— ▲ —)